# NAVIGATION AND SLIP KINEMATICS FOR HIGH PERFORMANCE MOTION MODELS

**Javier Hidalgo**

*DFKI - Robotics Innovation Center*
*Robert-Hooke-Str. 5, 28359 Bremen, Germany. Email: javier.hidalgo_carrio@dfki.de*

**ABSTRACT**

When absolute positioning systems are not available, kinematics modeling and rover chassis analyses play a dominant role in rover localization. It is the goal of this manuscript to describe and analyze a complete kinematic model which captures the six DoF pose (position and orientation) while traversing uneven terrains for hybrid systems and independently actuated wheels. The model is analyzed in order to correctly propagate rover pose as input for a pose estimator in localization towards efficient dead reckoning processes. Testing results are discussed for Asguard, a leg-wheel scout rover with a simple actuation system with enhanced maneuver capabilities.

Key words: robot motion, wheel odometry, rover kinematics, dead reckoning and planetary rovers.

## 1. INTRODUCTION

Typically dead-reckoning processes has been designed using indoor robotics experience and such inheritance has entailed simplified motion models with the typical planar assumption making considerable position errors, especially while traversing uneven terrains. This is critical, as dead-reckoning accumulates those errors over time. In order to find a solution, map building strategies and relative measurements are incorporated in a sensor fusion approach, usually SLAM, to correct them and therefore to reduce the pose uncertainty. Those techniques bring accurate solutions but might entail high memory usage and computational effort for planetary rovers with limited processing units on-board. Currently dead-reckoning solutions integrate sensor fusion scheme to minimize as much as possible the error. Kinematics modeling is the basic of probabilistic motion models which input the propagation step in such SLAM frameworks.

In general, rover kinematics plays fundamental roles in design, dynamic modeling, dead reckoning, vehicle control and wheel slip detection. As the control of hybrid systems is more complex, a motion model of the chassis is required to correctly command the desired trajectory and propagate the pose of the wheels as well as to reduce the slip by proper maneuvering [SSVO09]. Most efforts on kinematics have concentrated either on planar two-dimensional space, i.e., translation in the x-y plane and heading as the work in [Vol, GFASH09] or in more sophisticated systems with passive articulated joints [TM05]. Also active suspension systems have been recently analyzed in the literature [HC12].

Figure 1: The Asguard v3 platform developed at DFKI. It has mechanical properties similar to those of the Asguard v2 and includes additional sensors. The sensor suite includes a laser range finder, stereo camera, inertial measurement unit and a differential GPS for verification

Typically, the kinematics modeling can be solved by two methods, the geometric or the transformation approach. The geometric approach is more intuitive but it is restrictive to the particular platform lacking of generalization [ID04, GZM05, SH12]. The transformation approach is general and consistent by applying a series of transformations and Jacobian matrices to relate motion in the joint space to the Cartesian space, which main contribution is by Muir and Newman [MN86].

Extensive research with different reasoning is available in the literature. Alexander *et al* [AM89] present a planar rigid body model considering a variable number of wheels. Campion *et al* [CBDN96] classified ordinary mobile robots into five types taking into consideration

generic parts of the model equations. Other research into wheel-ground contact angle and pose estimation of robots moving on uneven surfaces can also be found in [LS07, ID00].

There are two main forms of locomotion for autonomous outdoor systems. Wheeled systems perform well in environments that contain roads or other flat surfaces. Legged systems are more complex, but can excel wheeled systems when it comes to unstructured terrain. Leg-wheel hybrid systems first developed at the ESA A&R group [MAdPH$^+$96] can combine some of the advantages of both domains. The Asguard system [JSK$^+$11] was developed at the DFKI and provides enhanced locomotion capabilities while maintaining mechanical simplicity. As of today, the challenges and problems of such hybrid structures have not been described in the literature and to the best of our knowledge no prior work exists that directly addresses this issue. The approach presented in this paper extends [TM05, MN86] in order to solve the complete kinematics of a hybrid leg-wheel rover. The methodology is applied to the particular case of Asguard v3 system depicted in Figure 1.

This manuscript starts by describing the hybrid leg-wheel kinematics model and its applicability to Asguard v3 system in Section 2. Different kinematics forms as the navigation kinematics (rover motion model) and the slip kinematics (wheel slip vector detection) are explained in Section 3. Experiments and test results are presented in Section 4 to finally conclude with a discussion of the methodology and future work.

## 2. LEG-WHEEL KINEMATICS MODELING

In the following the leg-wheel kinematics modeling is further described. Three main coordinate frames are defined: a robot body frame (*B*) attached to the desired rover center, a wheel axle (*A*) frame attached to the wheel axle and a wheel contact frame (*C*) defined as a single point of contact between the wheel and the ground (see Figure 2). The z-x plane of the (*A*) frame is aligned to the wheel plane and parallel with the z-x plane of the (*B*) frame when the rover is standing on a flat surface. The B frame is related to a fixed navigation-frame (*W*) by the pose vector $\boldsymbol{U} = \boldsymbol{u}_{W,B} = (x\ y\ z\ \phi\ \theta\ \psi)$. Each wheel frame $A_i = 0, 1, 2, ..., m_w - 1$ is related to the B frame by the transformation matrix $T_{B,A_i}(q)$ which depends on the particular chassis kinematics in joints space represented by the vector $\boldsymbol{q} = [q_1\ q_2\ ...\ q_{n-1}]$ where n is the number of degrees of freedom.

A key difference between typical mobile robots and hybrid leg-wheel systems is the point of contact (see Figure 3). Wheels cannot be considered to be a rigid disc in hybrid systems. This difference entails multiple transformations between the wheel axle *A*-frame and the wheel contact *C*. Multiple potential contact points $C_{ij}$ are defined where $i = 0, 1, 2, ..., m_w - 1$ is the number of wheels and $j = 0, 1, 2, ..., m_p - 1$ is the number of feet. Contrary to planar rovers, articulated rovers have a non-zero wheel contact angle $\delta_{ij}$. $\delta_{ij}$ defined at each *C*-frame

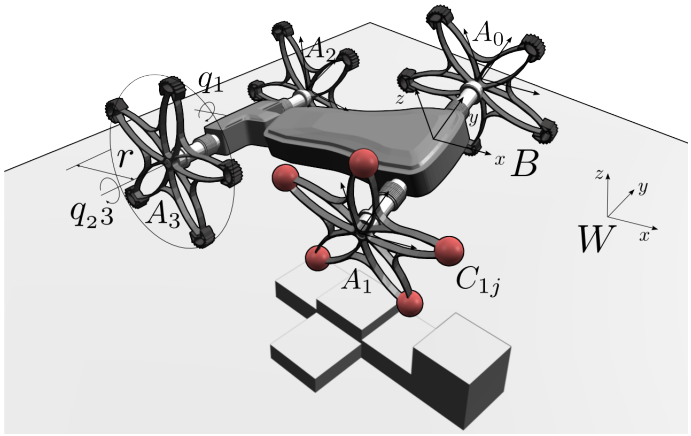


Figure 2: Illustration of Asguard rover kinematics modeling. $W$ is the world reference frame, $B$ is the body frame located in the center of the front axle, $A_i$ is the wheel axle frame and $C_{ij}$ the contact point frame. The pose estimation is computed as composition equation of wheel Jacobian matrices.

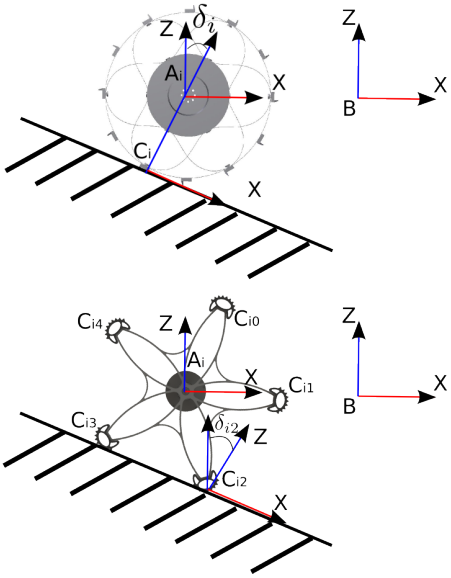


Figure 3: Schematic representation of coordinate frames for wheel $i$ on inclined terrain for conventional rigid disc (top) and hybrid leg-wheel systems (bottom). The contact angle is a key distinction between indoor and outdoor robots. While wheel's contact point is modeled in a constant location relative to the wheel axle in rigid disc, the assumption does not assign for a hybrid system.

as the angle between the normal vector to the terrain plane and the wheel z axis in *A*-frame. The contact angle is a key issue for hybrid leg-wheel rovers which their contact points define the direction of motion of the wheel.

$$T_{A_i,C_{ij}}(q_ni,\delta_{ij}) = \begin{bmatrix} c\delta_{ij} & 0 & s\delta_{ij} & rs(q_ni + j(2\pi/m_p)) \\ 0 & 1 & 0 & 0 \\ -s\delta_{ij} & 0 & c\delta_{ij} & rc(q_ni + j(2\pi/m_p)) \\ 0 & 0 & 0 & 1 \end{bmatrix} \quad (1)$$

The *C*-frame is related to the *A*-frame by the transformation matrix $T_{A_i,C_{ij}}(\delta_{ij})$ defined as a rotation of $\delta_{ij}$ along the y axis and a translation in z-axis defined by the wheel radius $r$ and the position of a specific foot point $j$. The corresponding transformation matrix is given in Equation 1 (where c denotes cosine and s sine):

The wheel forward kinematics solution relating the wheel contact point with respect to the body is defined by the matrix multiplication $T_{B,C_{ij}}(q,\delta_{ij}) = T_{B,A_i}(q)T_{A_i,C_{ij}}(q_ni,\delta_{ij})$. The motion of the contact point is composite from the slip vector modeled in three dimensions including a translation in the $x$ axis by $\xi_{ij}$, lateral slip $\eta_{ij}$ along the $y$ axis and rotational slip $\zeta_{ij}$ along the $z$ axis The resulting transformation matrix is (where $\bar{C}_{ij}$ is $C_{ij}(k-1)$ and $C_{ij}$ is $C_{ij}(k)$):

$$T_{\bar{C}_{ij},C_{ij}} = \begin{bmatrix} c\zeta_{ij} & -s\zeta_{ij} & 0 & \xi_{ij} \\ s\zeta_{ij} & c\zeta_{ij} & 0 & \eta_{ij} \\ 0 & 0 & 1 & 0 \\ 0 & 0 & 0 & 1 \end{bmatrix} \quad (2)$$

The transformation of the body frame *B* with respect to the wheel contact point frame including the slippage of the contact point is:

$$T_{\bar{C}_{ij},B} = T_{\bar{C}_{ij},C_{ij}}(\varepsilon_{ij})T_{C_{ij},A_i}(q_ni,\delta_{ij})T_{A_i,B}(q) \quad (3)$$

where $\varepsilon_{ij} = [\xi_{ij}\ \eta_{ij}\ \zeta_{ij}]$ is the slip vector at each specific contact point and the matrix $T_{C_{ij},A_i} = (T_{A_i,C_{ij}})^{-1}$ and $T_{A_i,B} = (T_{B,A_i})^{-1}$

Mobile robots are commonly commanded by desired velocities. The mapping between the rover Cartesian space rate vector $\dot{\boldsymbol{u}} = \dot{\boldsymbol{u}}_{\bar{B},B} = \begin{bmatrix}\dot{x}\ \dot{y}\ \dot{z}\ \dot{\phi}\ \dot{\theta}\ \dot{\psi}\end{bmatrix}$ and the joint space rate vector $\dot{q}$, the wheel rotation rate $\dot{q}_ni$, wheel slip rate vector $\dot{\varepsilon}_{ij}$ and the wheel-ground contact angle rate $\dot{\delta}_{ij}$ is solved by the Jacobian matrix. The velocity kinematics is deduced by applying the transformation matrix and the derivation of the point position relative to a coordinate system. Defining the transformation of the rover body at time step $k-1$ ($\bar{B}$) to rover body at time step $k$ ($B$) as $T_{\bar{B},B} = T_{\bar{B},\bar{C}_{ij}}T_{\bar{C}_{ij},C_{ij}}T_{C_{ij},B}$, the derivative is

$$\begin{aligned}\dot{T}_{\bar{B},B} = {} & \dot{T}_{\bar{B},\bar{C}_{ij}}T_{\bar{C}_{ij},C_{ij}}T_{C_{ij},B} + \\ & T_{\bar{B},\bar{C}_{ij}}\dot{T}_{\bar{C}_{ij},C_{ij}}T_{C_{ij},B} + \\ & T_{\bar{B},\bar{C}_{ij}}T_{\bar{C}_{ij},C_{ij}}\dot{T}_{C_{ij},B}\end{aligned} \quad (4)$$

Considering that for a general body in motion the position and orientation rates of $\dot{T}_{\bar{B},B}$ are defined by the skew matrix:

$$\dot{T}_{\bar{B},B} = \begin{bmatrix} 0 & -\dot{\psi} & \dot{\theta} & \dot{x} \\ \dot{\psi} & 0 & -\dot{\phi} & \dot{y} \\ -\dot{\theta} & \dot{\phi} & 0 & \dot{z} \\ 0 & 0 & 0 & 0 \end{bmatrix} \quad (5)$$

Equating matrices in Equation 4 and 5 the velocity kinematics is obtained. The equation can be reordered in order to have the wheel Jacobian matrix $J_{ij}$ associated to the contact point $j$ of the form

$$\begin{bmatrix}\dot{x}\ \dot{y}\ \dot{z}\ \dot{\phi}\ \dot{\theta}\ \dot{\psi}\end{bmatrix}^T = J_{ij}\begin{bmatrix}\dot{q}\ \dot{q}_ni\ \dot{\varepsilon}_{ij}\ \dot{\delta}_{ij}\end{bmatrix}^T \quad (6)$$

It defines the contribution of each wheel to the body rover motion allowing the analysis of each wheel and contact point to the resulting final velocity in $\dot{\boldsymbol{u}}$. The $J_{ij}$ matrix size is $6 \times (n+4)$ where $n$ corresponds to the DoF, which is the maximum number of DOFs in the kinematics chains between (*B*) frame and $C_{ij}$ frames. Finally, the composite rover equations are obtained combining the Jacobian matrices for all wheels into a sparse matrix equation as

$$\begin{bmatrix} I_6 \\ I_6 \\ \vdots \\ I_6 \end{bmatrix} \begin{bmatrix}\dot{x}\\ \dot{y}\\ \dot{z}\\ \dot{\phi}\\ \dot{\theta}\\ \dot{\psi}\end{bmatrix} = J \begin{bmatrix}\dot{q}\\ \dot{q}_n\\ \dot{\varepsilon}\\ \dot{\delta}\end{bmatrix} \equiv \qquad E\dot{u} = J\dot{p} \quad (7)$$

where $E$ is a $6m_w \times 6$ matrix that is obtained by stacking $m_w$ $6\times 6$ identity matrices, $\dot{q}$ is the $m_w(n-1)\times 1$ vector of rover joint angle rates, $\dot{q}_n$ is the $m_w \times 1$ vector of wheel rotation velocities, $\dot{\varepsilon}$ is the $3m_w \times 1$ slip vector and $\dot{\delta}$ is the $m_w \times 1$ vector of wheel-ground contact angle rates. The rover Jacobian matrix $J$ is a $6m_w \times (m_w n + 4m_w)$ matrix obtained from the individual leg-wheel Jacobian matrices $J_{ij}$. The vector $\dot{p}$ is a $(m_w n + 4m_w)\times 1$ vector of composite angular rates for $m_w$ wheels of the rover for the set of points in contacts $j = 0, 1, 2, ..., m_p - 1$.

| Name | Description | Dimension $(mm)$ |
|---|---|---|
| L | Wheel base distance | 510 |
| K | Half of track width | 267 |
| r | Average wheel radius | 197.5 |

Table 1: Asguard dimensions

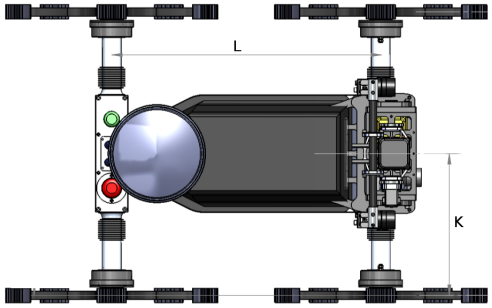


Figure 4: Representation of Asguard dimensions

## 3. ASGUARD KINEMATIC EQUATIONS

The rover kinematics just derived allow to estimate different quantities depending on the available sources and the specific quantities of interest. This article focuses on two forms since the purpose is to properly model hybrid leg-wheel system kinematics towards an efficient pose estimation during path following. This will be done by describing useful forms of Equation 7 for Asguard, referred as navigation kinematics and slip kinematics. Uncertainty modeling and step-integration is performed to estimate rover pose over time using dead reckoning methods. Other forms of interest as inverse kinematics and actuation kinematics to command desired rover velocities are also valuable to analyze, but they are beyond the scope of this paper.

Asguard is a simple yet highly capable hybrid system that is intended to serve as the scout rover unit in a multi-robot exploration scenario. It is able to navigate in complex uneven terrains and overcome demanding obstacles while maintaining a simple chassis mechanism. Asguard's front wheels have one single DoF to perform wheel rotation $q_1 i$. Asguard's rear wheels have two DoFs, one passive joint $q_1$ along the $x$ axis to freely adapt the rear part and the wheel rotation actuator $q_2 i$. Therefore, for the Asguard system DoFs $n = 2$. The transformation matrices from the body center to the front and rear wheels are found using the link values from Table 1 and depicted in Figure 4 as

$$T_{B,A_i} = \begin{bmatrix} 1 & 0 & 0 & 0 \\ 0 & 1 & 0 & (-1)^i K \\ 0 & 0 & 1 & 0 \\ 0 & 0 & 0 & 1 \end{bmatrix} \; i = 0, 1 \tag{8}$$

$$T_{B,A_i} = \begin{bmatrix} 1 & 0 & 0 & -L \\ 0 & c(q_1) & -s(q_1) & c(q_1)(-1)^i K \\ 0 & s(q_1) & c(q_1) & s(q_1)(-1)^i K \\ 0 & 0 & 0 & 1 \end{bmatrix} \; i = 2, 3 \tag{9}$$

The resulting transformation from Asguard body to the wheel contact point can be written as

$$T_{B,C_{ij}(q,\delta_{ij})} = T_{B,A_i}(q) T_{A_i,C_{ij}}(q_n i, \delta_{ij}) \;\; i = 0, 1, 2, 3 \tag{10}$$

It is noted that the contact point transformation depends on the articulated joints values $\boldsymbol{q}$ and the contact point angle $\delta_{ij}$. The Jacobian matrices are calculated as explained in Section 2 using Equation 10. The computation of the velocity kinematics requires the derivative of transformation matrices (cascade velocity derivative corollary [MN86]), which for Asguard rover is relatively simple since $T_{\bar{B},\bar{C}_{ij}}$ and $T_{\bar{C}_{ij},C_{ij}}$ are independent of time. The time derivative of $T_{\bar{B},B}$ has the form

$$\dot{T}_{\bar{B},B} = T_{\bar{B},\bar{C}_{ij}} T_{\bar{C}_{ij},C_{ij}} \dot{T}_{C_{ij},B} \tag{11}$$

The resulted $\dot{T}_{\bar{B},B}$ given by Equation 11 is equaled to the Equation 5 and the contact point Jacobian of the form in Equation 6 is obtained.

### 3.1. Navigation Kinematics

Navigation kinematics relates rover pose rate to the joints and sensed rate quantities. The navigation kinematics is the input for probabilistic motion models and is the basics for dead reckoning systems. The objective of the method is to estimate the rover pose and it is useful for the understanding of the role of different quantities contributing to the final rover pose.

The navigation kinematics focuses on the navigation form of Equation 11 when Asguard is rolling over its contact points and adapting to the uneven terrain. Joint angle measurements are available in Asguard rover through an absolute encoder installed in the passive joint and relative encoders available in all wheels. Asguard is also equipped with an IMU. The IMU only provides drift free measurement of pitch and roll angles. This is not totally possible by the heading error. Sensor availability defines sensed and not-sensed quantities and Equation 7 separates as

$$[E_s \quad E_n] \begin{bmatrix} \dot{u}_s \\ \dot{u}_n \end{bmatrix} = [J_s \quad J_n] \begin{bmatrix} \dot{p}_s \\ \dot{p}_n \end{bmatrix} \tag{12}$$

Rearranging into not-sensed (left-side) and sensed (right-side) quantities, the resulting equation is obtained

$$[E_n \quad -J_n] \begin{bmatrix} \dot{u}_n \\ \dot{p}_n \end{bmatrix} = [-E_s \quad J_s] \begin{bmatrix} \dot{u}_s \\ \dot{p}_s \end{bmatrix} \equiv A\chi = B\gamma \tag{13}$$

where $A$ and $B$ are matrices whose dimensions depend on the sensing capabilities of the rover system, and directly influence the existence of a solution. There is no solution if the matrix $A$ has not full-rank and therefore the system is undetermined. However, if $\mathrm{rank}[A|B] = \mathrm{rank}[A]$ the system is determined and a unique solution exits. When the system is overdetermined, $\mathrm{rank}[A|B] > \mathrm{rank}[A]$, there is more than one solution and least-squares is applied to solve the equations minimizing the error. If the matrix $A$ has fully-rank and $\mathrm{rank}[A|B] > \mathrm{rank}[A]$, there is ample sensing because it provides extra sensing capabilities. This extra information is very useful for error analysis and system design in early rover prototyping.

The passive joint angle and wheel rolling rates are sensed quantities, as well as the pitch $\dot{\phi}$, roll $\dot{\theta}$ and yaw $\dot{\psi}$ angles rates. The slip vector $\dot{\varepsilon}$ is not a sensed quantity and the contact point angles $\dot{\delta}$ are defined here as unknown values even though some techniques could be used to estimate these angles or by the installation of force sensors in the foot. Not-sensed quantities of the vector $\dot{u}$ are $\dot{x}$, $\dot{y}$ and $\dot{z}$. Here, the slip vector $\dot{\varepsilon}$ is modeled as only rotation along its z-axis $\zeta_i$ since it is assumed that the contact points slip with *nonholonomic* constraints. Therefore rows corresponding to the x and y-axis elements of the slip vector can be removed from the navigation kinematics. The resulting matrices $E_n$, $E_s$, $J_n$ and $J_s$ have dimensions $24 \times 3$, $24 \times 3$, $24 \times 5$ and $24 \times 8$ respectively. The matrix $A$ and $B$ have dimensions $24 \times 11$ and $24 \times 8$ respectively. The vector $\chi$ is a $11 \times 1$ vector corresponding to the not-sensed quantities, $\gamma$ is a $8 \times 1$ vector corresponding to the sensed quantities (i.e., Asguard passive joint, wheel rolling and angular velocities). The solution for the Equation 13 is obtained using least-squares where the error vector is given as

$$e = B\gamma - A\chi \tag{14}$$

the solution is based on minimizing the error vector $E = e^T C e$, where $C$ encodes the individual contribution of each wheel $i$ to the estimated solution. The matrix $C$ will be further discussed in Section 4. The solution to Equation 13 is given by

$$\chi = (A^T C A)^{-1} A^T C B \gamma \tag{15}$$

The desired quantities of Asguard pose $\dot{x}$ $\dot{y}$ $\dot{z}$ are extracted by taking the first element of the solution vector $\chi$. Least-squares solution provides an optimal solution by minimizing the error $e$ in velocity. This solution is applicable to dead reckoning methods. A large error represents larger navigation uncertainty, while a small error implies a more accurate solution.

### 3.2. Slip Kinematics

The detection of the slip vector $\varepsilon$ is important to identify the terrain, correct odometry errors and reduce undesirable motions. Similar to the navigation kinematics, the slip kinematics equation can be obtained per each leg-wheel. No-sensed values are worked out together at the left-side of the equation and sensed values are at the right-side

$$\begin{aligned} \begin{bmatrix} I_n & -J_{ijn} \end{bmatrix} \begin{bmatrix} \dot{\varepsilon}_{ij} \\ \dot{\delta}_{ij} \end{bmatrix} = \begin{bmatrix} -I_s & J_{ijs} \end{bmatrix} \begin{bmatrix} \dot{u} \\ \dot{q} \\ \dot{q}_{ni} \end{bmatrix} \\ A_{ij}\chi_{ij} = B_{ij}\gamma_i \\ i = 0,1,2,3 \quad j = 0,1,2,3,4 \end{aligned} \tag{16}$$

The analyses for the existence of a solution is similar to the navigation equations. The study the $\mathrm{rank}$ of $A_{ij}$ refers the sensing analysis of the slip equations. There is no solution if the matrix $A_{ij}$ has not full-rank and therefore the system is undetermined. The wheel slip rates could be fully detected if $\mathrm{rank}[A_{ij}|B_{ij}\gamma_i] = \mathrm{rank}[A_{ij}]$ or equivalent to express the residual error equal to zero as

$$A_{ij}(A_{ij}^T A_{ij})^{-1} A_{ij}^T - I B_{ij}\gamma_i \;=\; P(A_{ij}) - I B_{ij}\gamma_i = 0 \tag{17}$$

where $P(A_{ij})$ is the projection matrix to the column space of the matrix $A_{ij}$. When P is coincident with the identity matrix the error is zero and a unique solution exists for the slip vector. At this point, it is assumed that rover velocities $\dot{u}$ are know either using absolute positioning systems as GPS or visual odometry onboard. The wheel contact angle is unknown and the passive joint rate angles and wheel rolling rate are known. With this configuration the resulting matrices $I_s$ and $J_{ijn}$ have dimensions $6 \times 6$ and $6 \times 4$ and $J_{ijs}$ has dimensions $6 \times 1$ and $6 \times 2$ for front and rear wheels respectively. The matrix $A_{ij}$ and $B_{ij}$ have dimensions $6 \times 4$ and $6 \times 8$ or $6 \times 7$ respectively, with not-sensed vector $\chi_{ij}$ and sensed vector $\gamma_i$.

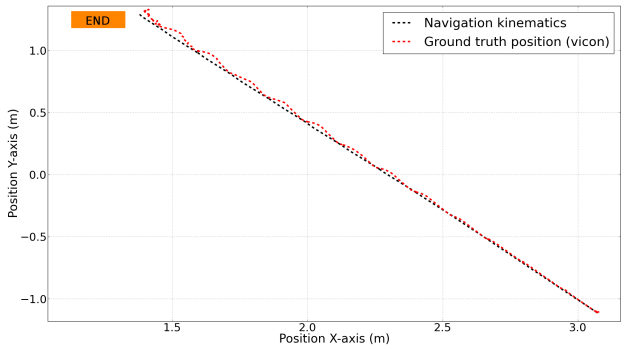


Figure 5: Straight line test for effective wheel radius calibration of the model.

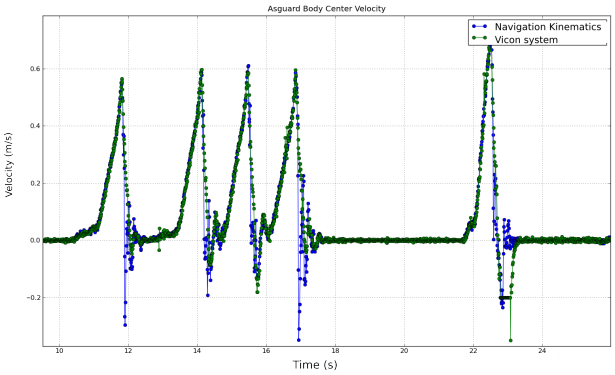


Figure 6: X-Forward Asguard body velocity during part of the straight line calibration test.

## 4. EXPERIMENTS

Experiments with the real hardware were performed. Controllable tests are required as a proof-of-concept in order to evaluate the feasibility of the approach and an indoor absolute tracking system is deployed in the Space Hall at DFKI. A set of seven infrared emitting and sensing cameras are mounted to the walls, which sense reflective markers mounted on the platform. These cameras are part of the Vicon system which can deduct and track position and orientation of objects equipped with such reflective markers. The deduced navigation kinematics as a key element of an accurate motion model and is compared with the typical planar assumption. Results for the slip kinematics are discussed and analyzed per each foot in contact.

### 4.1. Tests Results

Least-squares solution of the navigation kinematics is the minimum error solution for the rover velocities under wheel no-slip assumption. The dead reckoning update calculation is described as

$$\boldsymbol{U}(k) = \boldsymbol{U}(k-1) + \frac{\Delta t}{2} R_{W,\bar{B}}(\dot{\boldsymbol{u}}(k-1) + \dot{\boldsymbol{u}}(k)) \quad (18)$$

where $R_{W,\bar{B}}$ is a rotation matrix from $W$-frame to $\bar{B}$-frame. It is assumed that the rover motion is adequately modeled by constant accelerations since the robot is being actuated by constant force/torque generators in each sampling period $\Delta t$ (the same sampling period as the dead reckoning process). First, in order to calculate an effective wheel radius (Asguard has deformable rubber feet in all wheels) a straight line under non-slip conditions was performed. The resulting average wheel radius is the one in Table 1 and the final error is less than $1cm$ which is within the range of error for the Vicon system with this particular camera configuration (see Figure 5). The x-forward body velocity comparison between the proposed approach and the information given by the Vicon system is compared in Figure 6.

Figure 7 depicts the results for the serpentine path. All wheels slipped during the test due to the properties of the floor and types of maneuvers. Skid-steered mobile robots requires to slip along the wheel's contact points to perform certain maneuvers as point or skid turns.

It is important to note here the influence the weighting matrix has on the solution. The least-squares technique is very sensitive to the weight given to each wheel encodes in the matrix $C$. The weighting matrix codes the influence that each wheel contributes to the final solution. It should be the identity matrix for a well balanced rover driving on a flat surface. In the particular case of Asguard, the majority of the sensors are mounted closer to the front axle which brings the center of mass closer to the front wheels. The results are depicted in the zoom area of the serpentine trajectory (see figure 8). The weighting matrix gives a significant benefit for the Skid point turn maneuver bringing the center of rotation closer to the front axle. However, it is not that obvious at the last part of the trajectory where it is difficult to evaluate if the wheel weighting approach performs better. This is due to the fact that giving more importance to the front wheels also makes the solution more sensitive to the slippage of those wheels. Nevertheless, both approaches give more accurate solution than the conventional skid kinematics.

The dead reckoning integration is erroneous when wheel slip occurs and absolute positioning techniques are used to estimate the wheel slip vector described in Equation 16. Trajectories of the estimated wheel's contact points are shown in Figure 9.

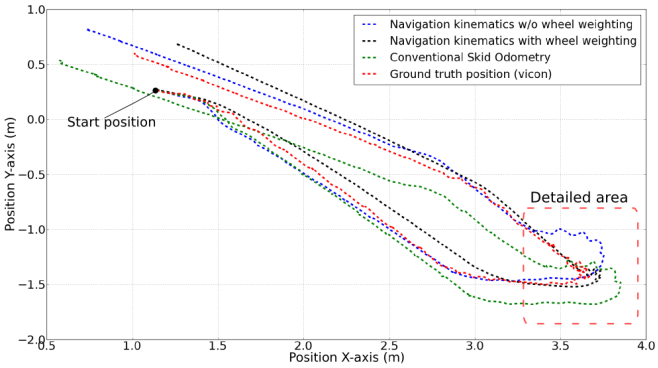


Figure 7: Serpentine slip test performed at DFKI Space hall. Two different navigation kinematics are compared depending on the weight assigned to each wheel for the resulting least-squares solution.

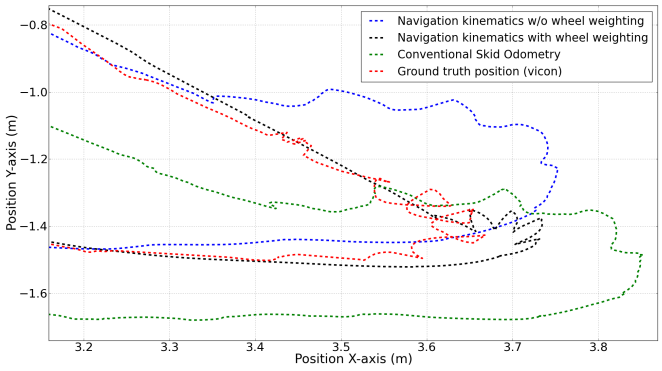


Figure 8: Detailed area of the point turn maneuver during the serpentine path. The navigation kinematics with the weighting matrix solution perform better in this case.

## 5. CONCLUSION

A methodology for the kinematic modeling and the pose estimation problem of a hybrid leg-wheel robot has been analyzed. The insight into kinematic modeling takes more importance for localization in the space sector where methods can not make use of the Global Positioning System (GPS). Therefore, a six DoF solution in a three dimensional space is desirable for positioning during complex maneuvers and long term navigation.

The following objectives have been achieved. (1) Calculation of the leg-wheel forward kinematics and Jacobian matrices for a general hybrid system. (2) Equations for the navigation and the slip kinematics for the Asguard rover. (3) Accurate results for dead-reckoning processes. (4) Analysis of the influence of a wheel weighting matrix.

Open questions arise after this work. The selection of the foot in contact with the ground is currently done by selecting the lowest $C_{ij}$ contact point with respect to the axle-frame $Ai$. Therefore, a more sophisticated technique is desirable to better estimate rover body velocity while negotiating big obstacles or climbing stairs. A precise weighting matrix which dynamically adjusts each wheel contribution according to rover's attitude is also interesting to evaluate. Finally, outdoors experiments in more challenging terrains as well as sensitivity analysis of the slip kinematics have especial interest in order to consolidate the benefit of the approach.

## ACKNOWLEDGMENTS

The author gratefully acknowledges the revision and comments of Dr. Sylvain Joyeux of DFKI RIC. The research described in this paper was performed within the ESA Networking Partnering Initiative (NPI), grant no. 4000103229/11/NL/P. This work has been supported in part by the IMPERA project, funded by the German Space Agency (DLR, Grant number: 50RA1111) with federal funds of the Federal Ministry of Economics and Technology (BMWi) in accordance with the parliamentary resolution of the German Parliament.

## REFERENCES

[AM89] J.C. Alexander and J.H. Maddocks. On the Kinematics of Wheeled Mobile Robots. *The International Journal of Robotics Research*, 8(5):15–27, October 1989.

[CBDN96] Guy Campion, Georges Bastin, and Brigitte D'Andrea-Novel. Structural Properties and Classification of Kinematic and Dynamic Models of Wheeled Mobile Robots. *IEEE Transactions on Robotics*, 12:47–62, 1996.

[GFASH09] P. Robuffo Giordano, M. Fuchs, A. Albu-Schaffer, and G. Hirzinger. On the kinematic modeling and control of a mobile platform equipped with steering wheels and movable legs. In *IEEE International Conference on Robotics and Automation*, pages 4080–4087. Ieee, May 2009.

[GZM05] Bernd Gassmann, Franziska Zacharias, and J Z Marius. Localization of Walking Robots. In *IEEE International Conference on Robotics and Automation*, number April, pages 1471–1476, 2005.

[HC12] Javier Hidalgo and Florian Cordes. Kinematics Modeling of a Hybrid Wheeled-Leg Planetary Rover. In *International Symposium on Artificial Intelligence, Robotics and Automation in Space*, 2012.

[ID00] K. Iagnemma and S Dubowsky. Vehicle Wheel-Ground Contact Angle Estimation: with Application to Mobile Robot Traction Control. In *International Symposium on Advances in Robot Kinematics*, pages 137 – 146, 2000.

[ID04] K. Iagnemma and S Dubowsky. *Mobile Robots in Rough Terrain: Estimation, Motion Planning, and Control with Application to Planetary Rovers*, volume 12. 2004.

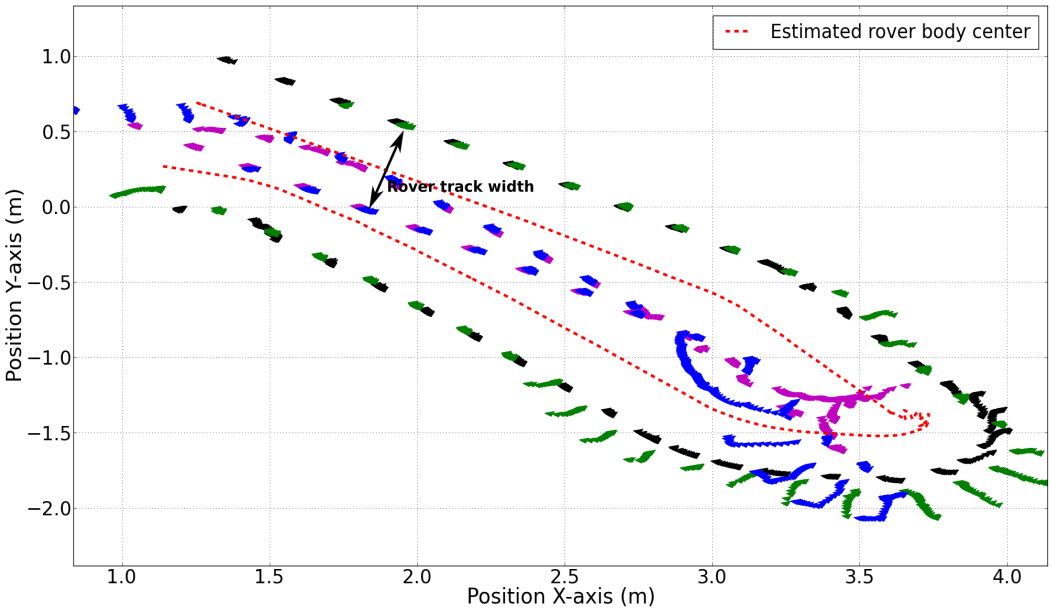


Figure 9: Slip map for the serpentine test performed at DFKI Space hall. Front left wheel contact points are depicted in magenta, front right in black, rear left in blue and rear right in green color.


[JSK+11] Sylvain Joyeux, Jakob Schwendner, Frank Kirchner, Ajish Babu, Felix Grimminger, Janosch Machowinski, Patrick Paranhos, and Christopher Gaudig. Intelligent Mobility - Autonomous Outdoor Robotics at the DFKI. *KI - Kuenstliche Intelligenz*, February 2011.

[LS07] P. Lamon and R. Siegwart. 3D Position Tracking in Challenging Terrain. *The International Journal of Robotics Research*, 26(2):167–186, February 2007.

[MAdPH+96] A. Martin-Alvarez, W. de Peuter, J. Hillebrand, P. Putz, A. Matthyssen, and J. F. de Weerd. Walking Robots for Planetary Exploration Missions. In *Second World Automation Congress*, 1996.

[MN86] Patrick F Muir and Charles P Neuman. *Kinematic Modeling of Wheeled Mobile Robots*. Number June. 1986.

[SH12] Jakob Schwendner and Javier Hidalgo. Terrain aided navigation for planetary exploration missions. In *International Symposium on Artificial Intelligence, Robotics and Automation in Space*, pages 1 – 8, 2012.

[SSVO09] Bruno Siciliano, Lorenzo Sciavicco, Luigi Villani, and Guiseppe Oriolo. *Robotics. Modeling, Control and Planning*. 2009.

[TM05] Mahmoud Tarokh and Gregory J Mcdermott. Kinematics Modeling and Analyses of Articulated Rovers. *IEEE Transactions on Robotics*, 21(4):539–553, 2005.

[Vol] R. Volpe. Inverse Kinematics for All-Wheel Steered Rovers. Technical report.